DTIC

AFRL-MN-EG-TP-2005-7405

Preliminary Development of a Computational Model of a Dielectric Barrier Discharge

Maj William M. Hilbun
Air Force Research Laboratory
Munitions Directorate
AFRL/MNAC
Eglin AFB, FL 32542-6810

Benjamin J. Case
SENTEL Corporation
TEAS IV Group
Eglin AFB, FL 32542-6810

DECEMBER 2004

This work has been submitted to the American Institute of Aeronautics and Astronautics for presentation at, and publication in proceedings of, the 43rd AIAA Aerospace Sciences Meeting and Exhibit, 10-13 Jan 2005, Reno, NV.

AIR FORCE RESEARCH LABORATORY, MUNITIONS DIRECTORATE

Air Force Materiel Command ■ United States Air Force ■ Eglin Air Force Base

REPORT DOCUMENTATION PAGE

Form Approved OMB No. 0704-0188

1. REPORT DATE *(DD-MM-YYYY)*	2. REPORT TYPE	3. DATES COVERED *(From - To)*
04-Dec-2004	Conference Paper Preprint	

4. TITLE AND SUBTITLE
Preliminary Development of A Computational Model of a Dielectric

5a. CONTRACT NUMBER

5b. GRANT NUMBER

5c. PROGRAM ELEMENT NUMBER
61102F

6. AUTHOR(S)
Maj William M. Hilbun –AFRL/MNAC

Benjamin J. Case – SENTEL Corp., TEAS IV Group

5d. PROJECT NUMBER
2302 & 2307

5e. TASK NUMBER
BN & BN

5f. WORK UNIT NUMBER
01 & 05

7. PERFORMING ORGANIZATION NAME(S) AND ADDRESS(ES)

Air Force Research Laboratory
Munitions Directorate
AFRL/MNAC
Eglin AFB, FL 32542-6810

SENTEL Corporation
TEAS IV Group
Eglin AFB, FL 32542-6810

8. PERFORMING ORGANIZATION REPORT NUMBER

9. SPONSORING / MONITORING AGENCY NAME(S) AND ADDRESS(ES)
Air Force Research Laboratory
Munitions Directorate
AFRL/MNAC
Eglin AFB, FL 32542-6810

10. SPONSOR/MONITOR'S ACRONYM(S)
AFRL-MN-EG

11. SPONSOR/MONITOR'S REPORT NUMBER(S)
AFRL-MN-EG-TP-2005-7405

12. DISTRIBUTION / AVAILABILITY STATEMENT
APPROVED FOR PUBLIC RELEASE; DISTRIBUTION UNLIMITED

13. SUPPLEMENTARY NOTES This work has been submitted to the American Institute of Aeronautics and Astronautics for presentation at, and publication in proceedings of, the 43rd AIAA Aerospace Sciences Meeting and Exhibit, 10-13 Jan 2005, Reno, NV. One of the authors is a U.S. Government employee working within the scope of his position; therefore, the U.S. Government is joint owner of the work. It published, American Institute of Aeronautics and Astronautics may assert copyright. If so, the Government has the right to copy, distribute, and use the work. Any other form of use is subject to copyright restrictions.

14. ABSTRACT
A 1D model of a plasma actuator has been developed. The plasma actuator is modeled as a dielectric barrier discharge (DBD) and is based on the numerical solution of the electron and ion conservation of mass and momentum equations, in the drift-diffusion regime, coupled with the Poisson equation for the self-consistent calculation of the electric field. An analytic representation of the force density on the neutral gas due to the presence of a plasma is derived, which is applicable within the drift-diffusion regime. The code is validated by comparison to previous calculations and then applied to a series of test problems to examine the behavior of the plasma force density.

15. SUBJECT TERMS
Plasma; plasma flow; neutral flow; neutral gas; transient plasma; electron momentum; DC glow discharge

16. SECURITY CLASSIFICATION OF:			17. LIMITATION OF ABSTRACT	18. NUMBER OF PAGES	19a. NAME OF RESPONSIBLE PERSON
a. REPORT	b. ABSTRACT	c. THIS PAGE			Steven Ellison
Unclassified	Unclassified	Unclassified	Unlimited	22	19b. TELEPHONE NUMBER *(include area code)* 850-882-8302

Preliminary Development of a Computational Model of a Dielectric Barrier Discharge

William M. Hilbun, Major, USAF*
US Air Force Research Laboratory
Eglin AFB FL 32542-6810

Benjamin J. Case†
SENTEL Corp., TEAS IV Group
Eglin AFB FL 32542-6810

A 1D model of a plasma actuator has been developed. The plasma actuator is modeled as a dielectric barrier discharge (DBD) and is based on the numerical solution of the electron and ion conservation of mass and momentum equations, in the drift-diffusion regime, coupled with the Poisson equation for the self-consistent calculation of the electric field. An analytic representation of the force density on the neutral gas due to the presence of a plasma is derived, which is applicable within the drift-diffusion regime. The code is validated by comparison to previous calculations and then applied to a series of test problems to examine the behavior of the plasma force density.

D = Diffusivity coefficient, m^2/s
E = Electric field, V/m
L = Time rate of change of particle density due to loss processes, $m^{-3} s^{-1}$
P = Pressure, torr
S = Time rate of change of particle density due to production processes, $m^{-3} s^{-1}$
T = Temperature, K

e = Elementary charge, C
k_B = Boltzmann constant, J/K
m = Mass, kg
n = Number density, m^{-3}
t = Time, s
v = Velocity, m/s

Γ = Particle flux, $m^{-2} s^{-1}$
Φ = Electric potential, V
ε = Permittivity coefficient, F/m
μ = Mobility coefficient, $m^2 V^{-1} s^{-1}$
ν = Frequency, s^{-1}
ρ = Density, kg/m^3

I. Introduction

Aerodynamic flow control by means of plasma actuators is currently an active area of research. Such devices have experimentally demonstrated their ability to reattach separated flow at high angles of attack[1, 2, 3] as well as to induce flow movement in an initially stationary air mass[4, 5]. The use of plasma actuators in such a role may offer several advantages over traditional flow control devices (e.g., slats, flaps, slots). Some of these advantages may be

- Reduced size and weight
- Increased reliability[6]
- Increased aerodynamic agility
- Reduced drag[7]
- High bandwidth[8]
- No moving parts (leading to improved manufacturability)[9]

---

* Computational Physicist, Munitions Directorate, AFRL/MNAC, 101 W. Eglin Blvd, Member AIAA.
† Aeronautical Engineer, 308 West D Ave., Member AIAA

- Inexpensive[10]
- No tail fins (leading to increased weapon load out of combat aircraft)[9]

Plasma flow control devices will, no doubt, have disadvantages in comparison to traditional flow control devices as well. For example, plasma actuators may not perform well in adverse weather conditions and will require electrical power to operate, although it has been shown that this latter requirement can be mitigated through a "smart" actuator methodology.[11]

Whether plasma actuators offer any demonstrable advantages over traditional flow control methodologies remains to be seen. However, in order to exploit such devices to the fullest extent possible, it is necessary to have a basic understanding of the physical phenomena upon which they are based. Although the experimental component of plasma actuator research has made significant discoveries, the modeling and simulation of these devices has been conspicuously lacking. It is the aim of the present paper to aid in this respect through careful computational modeling of the relevant physics describing the heart of a plasma actuator, the dielectric barrier discharge (DBD).

II. Physical Model

In order to quantify the effect of the plasma on the neutral flow momentum, a suitable momentum transfer model must be adopted. The model proposed in this work is given as

$$\frac{\partial \rho_n \vec{v}_n}{\partial t} + \vec{\nabla} \cdot \rho_n \overleftrightarrow{v_n v_n} = -\vec{\nabla} P_n + \sum_{s=e,i} \rho_s \nu_{sn} (\vec{v}_s - \vec{v}_n) \tag{1}$$

where the last term on the right represents the time rate of momentum transfer per unit volume (i.e., force density) from electrons and ions to the neutrals, through collisions.[12] In an analogous fashion the ion momentum equation can be modeled as

$$\frac{\partial \rho_i \vec{v}_i}{\partial t} + \vec{\nabla} \cdot \rho_i \overleftrightarrow{v_i v_i} = -\vec{\nabla} P_i + n_i e \vec{E} - \rho_i \nu_{in} (\vec{v}_i - \vec{v}_n) \tag{2}$$

where the second term on the right describes momentum gained by the ions due to the electric field and the last term on the right represents momentum lost by the ions due to collisions with the neutrals. A similar equation can be written for the electrons. The simplest model describing the relevant physics of a DBD is based on the drift-diffusion model of a plasma. In this model, the formal solution of Eq. (2) is avoided by instead solving "pseudo-algebraic" momentum equations for each species. These algebraic equations are derived by neglecting the inertial terms resulting in a balance between the electrical force, the pressure gradient force, and the collisional momentum transfer term. Thus, the ion velocity may be approximated as

$$\vec{v}_i = \vec{v}_n + \frac{e\vec{E}}{m_i \nu_{in}} - \frac{\vec{\nabla} P_i}{\rho_i \nu_{in}} \tag{3}$$

with a similar result for the electron velocity. Substituting these expressions into the neutral momentum equation leads to

$$\frac{\partial \rho_n \vec{v}_n}{\partial t} + \vec{\nabla} \cdot \rho_n \overleftrightarrow{v_n v_n} = -\vec{\nabla} P_n - \vec{\nabla} P_e - \vec{\nabla} P_i + (n_i - n_e) e \vec{E} \tag{4}$$

or

$$\frac{\partial \rho_n \vec{v}_n}{\partial t} + \vec{\nabla} \cdot \rho_n \overleftrightarrow{v_n v_n} = -\vec{\nabla} P_n + \vec{F}_{plasma} \tag{5}$$

with

$$\vec{F}_{plasma} = -\vec{\nabla}P_e - \vec{\nabla}P_i + (n_i - n_e)e\vec{E} \tag{6}$$

Thus, Eq. (6) defines the force density on the neutral gas due to the presence of a plasma. The presence of the plasma adds momentum to the neutral gas in three ways: via an electron pressure gradient, via an ion pressure gradient, and via an electric field term. The last term on the right hand side of Eq. (6) is exactly the same as that given by Enloe, et al (Ref. 4). The electron and ion pressure gradient source terms, while not previously reported in the plasma actuator literature, can be shown to be negligible for operating conditions that are typical for a DBD at atmospheric pressure.

The rest of the plasma drift-diffusion model consists of the equations describing conservation of mass for the electrons and ions

$$\frac{\partial n_{e,i}}{\partial t} + \vec{\nabla}\cdot(\vec{\Gamma}_{e,i}) = S_{e,i} - L_{e,i} \tag{7}$$

and Poisson's equation which describes the electric potential

$$\nabla^2\Phi = -\frac{e}{\varepsilon}(n_i - n_e) \tag{8}$$

The electric field and the potential are related by

$$\vec{E} = -\nabla\Phi \tag{9}$$

Returning to Eq. (2) and assuming an initially stationary neutral gas and a constant ion temperature, the ion flux can be defined as

$$\vec{\Gamma}_i = n_i\mu_i\vec{E} - D_i\vec{\nabla}n_i \tag{10}$$

where D is the diffusion coefficient, defined as

$$D_i = \frac{kT_i}{m_i\nu_{in}} \tag{11}$$

and μ is the mobility coefficient, defined as

$$\mu_i = \frac{e}{m_i\nu_{in}} \tag{12}$$

In a similar fashion, the electron flux is defined as

$$\vec{\Gamma}_e = -n_e\mu_e\vec{E} - D_e\vec{\nabla}n_e \tag{13}$$

In the simplest approaches, it is assumed that the relevant diffusion and mobility coefficients, along with the mass production (S) and loss terms (L), can be accurately modeled as functions of the reduced electric field (E/N, where N is the neutral number density). In order for this assumption to be valid, local equilibrium must exist for each species.[13] Equilibrium conditions will exist if the characteristic time for the electrons to reach a steady-state energy

distribution is small compared to the characteristic time for the discharge to develop. This is considered to be the case for DBDs at atmospheric pressure and this modeling approach has been widely used.[14,15,16,17,18,19]

In summary, the plasma drift-diffusion model consists of the set of Eqs. (7), (8), and (9) with the ion and electron fluxes given by Eqs. (10) and (13), respectively. In principle, the solution of the plasma drift-diffusion equations could be coupled with a simultaneous solution of the neutral gas momentum in order to accurately determine the effect of the plasma on the neutral flow. In practice this is made difficult by the disparate time scales corresponding to the plasma actuator and the neutral flow. For example, a typical plasma actuator has a length of approximately 1 cm and induces a neutral flow velocity of approximately 3 m/s,[20] resulting in a characteristic time for the neutral gas on the order of 3 ms. On the other hand, the DBD plasma actuator typically operates at a frequency of 5-10 kHz, which corresponds to a characteristic time of 0.1-0.2 ms, or a factor of 15-30 times faster than the neutral flow. This difference in time scales suggests that the effect of the plasma on the neutral gas can be modeled by averaging the body force term in Eq. (5) over one period (T) of the DBD:

$$\vec{F}_{plasma}(\vec{x}) \approx \left\langle \vec{F}_{plasma}(\vec{x},t) \right\rangle = \frac{\int_0^T [-\vec{\nabla}P_e(\vec{x},t) - \vec{\nabla}P_i(\vec{x},t) + (n_i(\vec{x},t) - n_e(\vec{x},t))e\vec{E}(\vec{x},t)]\,dt}{T} \tag{14}$$

In this manner, the plasma equations are decoupled from the neutral flow equations, and the effect of the plasma can be accounted for by an average body force term in the neutral gas momentum equation. This force term depends on position but is independent of time.

At this point it must be mentioned that the typical plasma actuator is inherently at least a two-dimensional device, and care has correspondingly been taken in writing all the equations presented to this point in order to retain their dimensionality. However, the present work to date has been limited to a single dimension to examine the physics in their simplest setting, and to allow for a systematic numerical building block approach. Several researchers have pointed out the difficulties involved in capturing the correct physics with a one-dimensional approach,[15,16,21] particularly with regard to the calculation of the electric field. Further note of this will be made where appropriate.

III. Numerical Scheme

The system of equations (7, 8, 9) is highly nonlinear and stiff, and therefore numerically difficult to solve. The numerical scheme implemented in this work has been adapted from that of Boeuf,[22] and uses an implicit difference representation based on the exponential discretization method of Scharfetter and Gummel.[23] This technique, originally developed for simulations of electron and hole transport in semiconductors, is robust, stable, and able to deal with situations where either the field driven flux (first term in Eq. [13]) or the diffusive flux (second term in Eq. [13]) is dominant. The former is dominant near electrodes while the latter is dominant in the quasi-neutral plasma region.

The temporal integration of the system of equations is performed by successively solving the Poisson equation (assuming the particles do not move), followed by solving the charge continuity equations (assuming the electric field does not change), as can be seen in Fig. 1. Thus, although the continuity equations are solved implicitly in time, the overall temporal integration scheme is explicit in nature.

The integration of the continuity equations uses a simple forward difference for the time derivative of the number density and a central implicit difference for the spatial derivative of the flux:

$$\frac{n_i^{k+1} - n_i^k}{\Delta t} + \frac{\Gamma_{i+1/2}^{k+1} - \Gamma_{i-1/2}^{k+1}}{\Delta x} = S_i^k \tag{15}$$

with the source term evaluated explicitly, as shown.

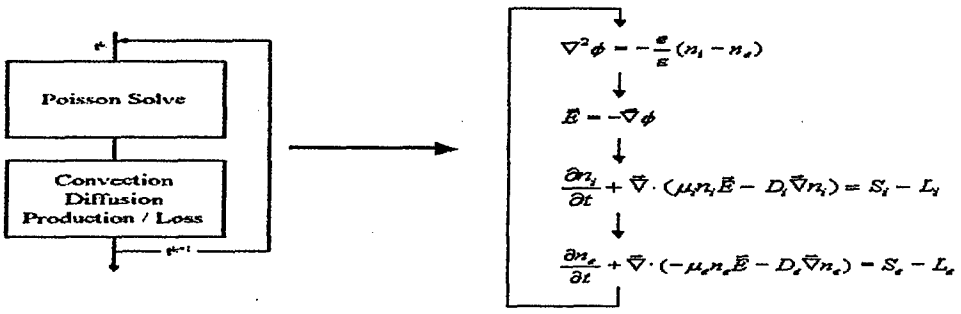

Figure 1. Overall time integration methodology.

The Scharfetter/Gummel exponential spatial discretization is used to represent the fluxes:

$$\Gamma_{i+1/2}^{k+1} = \frac{1}{\Delta x}\left[n_i^{k+1} D_i^k \exp(Z_{i+1/2}^k) - n_{i+1}^{k+1} D_{i+1}^k\right] \frac{Z_{i+1/2}^k}{\exp(Z_{i+1/2}^k) - 1} \tag{16}$$

where

$$Z_{i+1/2}^k = -s\frac{\mu_{i+1/2}^k}{D_{i+1/2}^k}\left(\Phi_{i+1}^k - \Phi_i^k\right) \tag{17}$$

where s is equal to –1 for negatively charged particles and +1 for positively charged particles. Note that the number densities are evaluated at time $k + 1$, while all other quantities are evaluated at time k. Note also that Z is unitless, as it should be.

The main advantage of this scheme is that it provides a numerically stable representation of the electron and ion flux under either field-dominant or diffusion-dominant conditions. Representing the flux using a standard finite difference approximation leads to numerical instabilities when the electric potential between adjacent cell nodes is of the order or larger than the characteristic energy (given by Einstein's relation as $D/\mu = k_B T/e$).[22] On the other hand, it can be shown that use of the present method reduces the discretized PDE of Eq. (15) to a diffusion equation (of second-order accuracy) for a diffusion-dominated flux, and to a convection equation (with upwinding) for a field-dominated flux.

The grid is defined such that equally spaced nodes are located throughout the interior of the plasma domain (Fig. 2), with cell interfaces located halfway between cell nodes. Number densities and electric potential are defined on the cell nodes, while the fluxes are evaluated at the cell interfaces. At the boundaries of the plasma domain, the grid is modified in order to place the boundary at a cell interface (Fig. 3). This methodology has useful conservation properties[24] and makes the boundary conditions particularly easy to implement.

Figure 2. Discretization of the computational domain.

Discretizing the fluxes according to the Scharfetter/Gummel prescription results in a tridiagonal system of equations,

$$A_i^k n_{i-1}^{k+1} + B_i^k n_i^{k+1} + C_i^k n_{i+1}^{k+1} = D_i^k \tag{18}$$

which is efficiently solved in O(3N) operations using a concisely coded procedure based on LU decomposition with forward and back substitution.[25]

Boundary conditions must be applied to the number densities and fluxes of both species at the edges of the plasma domain. Accordingly, the normal gradient of the number density is required to be zero at a boundary for those cases in which the electric field at the boundary would normally drive particles out of the plasma domain. Therefore, the boundary condition for outgoing particle flux is given simply by Eq. (10) (reduced to a field driven flux only, since $\vec{\nabla} n = 0$). If the boundary for the outgoing particles is a dielectric surface, the flux is integrated in time in order to calculate the surface charge density. The incoming flux for positive ions is set to zero for those cases in which the electric field at the boundary points into the plasma domain. The incoming flux boundary condition for electrons depends upon whether the boundary is an electrode or a dielectric surface. At an electrode boundary, the incoming electron flux is defined to be a fraction of the outgoing positive ion flux at the same location (but opposite in sign), i.e.,

$$\vec{\Gamma}_e = -\gamma \vec{\Gamma}_i \tag{19}$$

where γ is defined as the secondary ionization coefficient (with values typically between 0 and 0.5). At a dielectric boundary the incoming flux is described by

$$\vec{\Gamma}_e = \sigma_e \nu_e^{desorption} \hat{n} - \gamma \vec{\Gamma}_i \tag{20}$$

where $\nu_e^{desorption}$ is the desorption frequency for the electrons leaving the dielectric surface, and $\hat{n}$ is a unit vector pointing into the plasma domain. This description is similar to that reported by Golubovskii.[26]

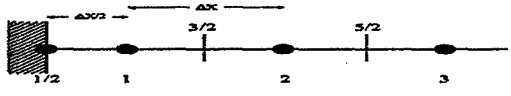

Figure 3. Discretization of the computational domain near a boundary.

Poisson's equation is discretized with a second-order central finite difference representation, and solved using a point Gauss-Seidel method with successive over-relaxation. In practice this method converges in a few thousand iterations for the initial transient, thereafter converging in only a few iterations per time step.

For cases in which a dielectric barrier is present, Laplace's equation is solved in the interior of the dielectric and a constraint condition, derived from Gauss's law, is placed on the normal component of the electric field at the plasma/dielectric interface:

$$\left.\frac{\partial \Phi}{\partial x}\right|_{plasma} = \frac{\varepsilon_{dielectric}}{\varepsilon_{plasma}} \left.\frac{\partial \Phi}{\partial x}\right|_{dielectric} \pm \frac{\sigma}{\varepsilon_{plasma}} \tag{21}$$

The plus sign is used for 1D configurations in which the dielectric is to the right of the plasma, and the minus sign for when the dielectric is to the left of the plasma. The constraint condition is included as part of an iterative solution for the potential within the entire spatial domain. That is, Poisson's equation and Laplace's equation are alternately solved in the plasma and dielectric domain (respectively), while a discretized version of Eq. (21) is used to define an updated value of the potential on the dielectric interface with each cycle. This process is repeated until the solution through the entire domain converges.

In the explicit time integration approach, in which successive solutions are found for the continuity and Poisson's equation, the time step is constrained to be less than corresponding dielectric relaxation time[27, 28] given by

$$t_d = \frac{\varepsilon_0}{e(\mu_e n_e + \mu_i n_i)} \tag{22}$$

IV. Validation

A. Transient Plasma Sheath for a Negative Potential

As a first test of the coupled plasma/potential solver, the case of a sheath in a non-ionizing Argon plasma at a pressure of 100 torr is examined.[29] The transport parameters used are as given as

$$\mu_e = 0.3 \quad \mathrm{m^2/Vs} \qquad D_e = 0.3 \quad \mathrm{m^2/s}$$
$$\mu_i = 10^{-3} \quad \mathrm{m^2/Vs} \qquad D_i = 10^{-4} \quad \mathrm{m^2/s}$$

These parameters define characteristic temperatures, based on the Einstein relation, for the electrons and ions of 1 eV and 0.1 eV, respectively. The left boundary of the domain is an electrode, initially at a potential of 0 V. The right boundary models a free plasma region a distance of 200 characteristic Debye lengths (λ_{D0}, based on conditions in the unperturbed bulk plasma) from the left boundary. The electron and positive ion densities are spatially uniform at time $t = 0$, while the electric potential is initially zero throughout the domain. In the results that follow, the various quantities have been nondimensionalized by their characteristic values: number densities by n_{e0}, electric potential by $\Phi_0 = k_B T_e / e$, electric field by $E_0 = \Phi_0 / \lambda_{D0}$, the force density by $F_0 = e n_{e0} E_0$, and time by the dielectric relaxation time considering only the ions (t_{di}). At time $t = 0$ the left electrode is instantaneously brought to a nondimensional potential of –50. The sudden application of a negative potential forces the highly mobile electrons away from the electrode, while the positive ions are attracted to the electrode. As the charges separate an induced electric field arises, which attempts to neutralize the total field (applied + induced) within the bulk of the plasma.

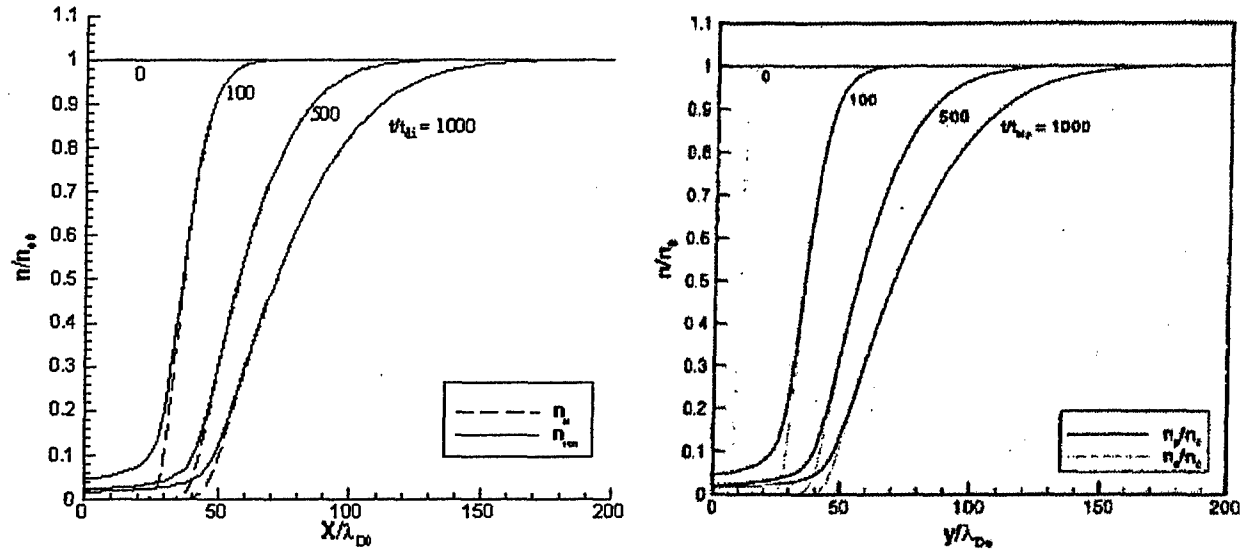

(a) Present calculation

(b) Previous calculation (Ref. 29)

Figure 4. Normalized electron and ion number densities as a function of distance away from the electrode for test case 1. (b) Results from a previous calculation (Ref. 29) under the assumption that the electrons are in equilibrium with the electric potential. (a) Results from the present calculation, which makes no such assumption.

A comparison of number densities between the present effort and previous work (Ref. 29) is highlighted in Fig. 4, which shows excellent agreement. The time units have been normalized according the dielectric relaxation time corresponding only to the ions (i.e., t/t_{di}), in order to make an equal comparison. The actual calculation was made based on the relaxation time given by Eq. (22), which is governed by the electrons. A key difference between Ref. 29 and the present effort lies in the treatment of the electrons. In the previous work, the electron continuity equation was not solved; instead the electrons were assumed to be in equilibrium with the electrical potential throughout the domain, with the number density defined according to the Maxwell-Boltzmann distribution:

$$n_e(\Phi) = n_{eo} \exp\left(\frac{e\Phi}{k_B T_e}\right) \tag{23}$$

This assumption is identical to neglecting the inertial and collision terms in the electron momentum equation, and balancing the electrical force with the electron pressure gradient. In the present work, this assumption is not made; both the ion and electron continuity equations are solved simultaneously. A major consequence of this is that at $t \approx 0$ (just after the normalized potential at the left electrode becomes –50, but before the electrons and ions can redistribute themselves to cancel out the total electrical field in the bulk plasma) a uniform electric field exists throughout the domain (see Fig. 5a for $t/t_{mp} = 1$). This field acts to drive all electrons to the right and all ions to the left. Thus, electrons at the right edge of the computational domain are lost to the bulk plasma, while positive ions in the bulk plasma are added to the computational domain. The highly mobile electrons quickly redistribute themselves in such a way as to cancel out the electrical field in the bulk plasma. The time scale for this process is on the order of several tens of dielectric relaxation times, as given by Eq. (22).

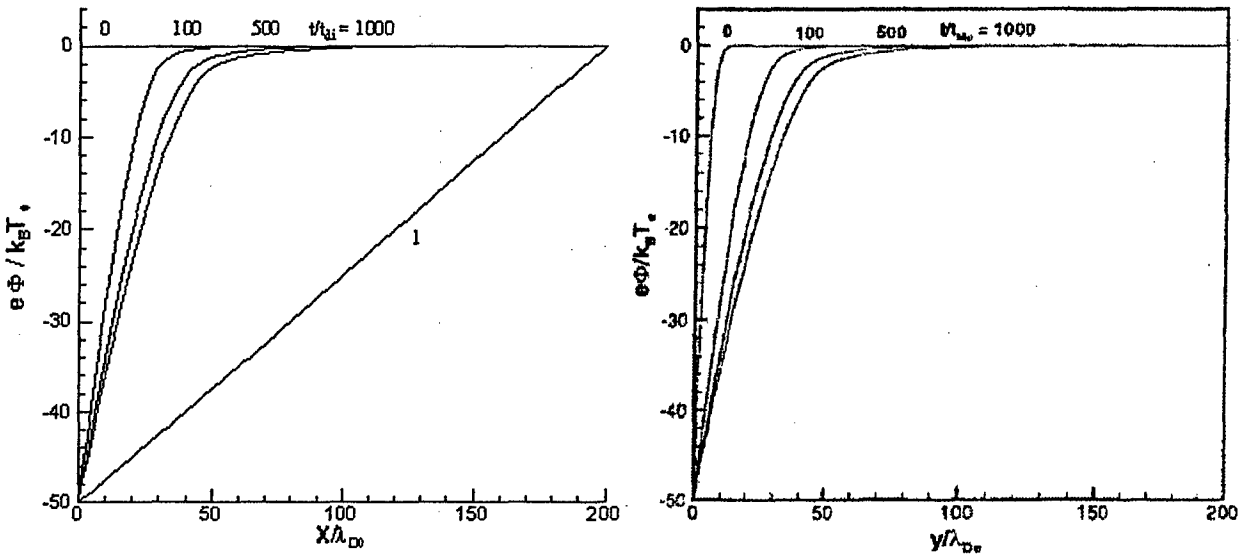

(a) Present calculation (b) Previous calculation (Ref. 29)

Figure 5. Electric potential throughout the domain for test case 1. (b) Results from a previous calculation (Ref. 29) under the assumption that the electrons are in equilibrium with the electric potential. (a) Results from the present calculation, which makes no such assumption.

The charged particle densities, electric potential, and electric field are shown in Fig. 6a at time $t/t_{di} = 100$. Near the cathode ($x = 0$) the electric field is negative, and there is a region of net positive charge. The corresponding components of the plasma force density on the neutral gas (i.e., Eq. [6]) are also shown (Fig. 6b). In this case of a sheath in a negative potential, (i.e., one in which the sheath is located in a potential that is lower than that of the bulk plasma) it is observed that all three components of the plasma force are negative and that the force due to the electron density gradient can be significant at this low value of potential. At higher values of applied potential, the force due to the density gradients becomes negligibly small in comparison to the electric force.

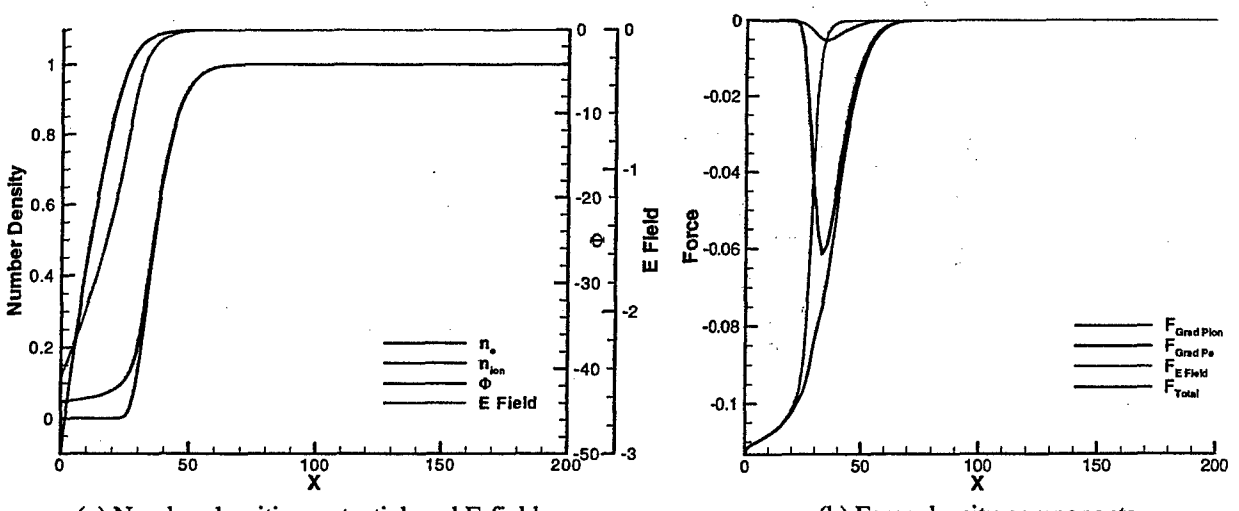

(a) Number densities, potential, and E-field (b) Force density components

Figure 6. Results from a plasma sheath in a negative potential at 100 nondimensional time units. All quantities have been appropriately nondimensionalized.

A space-time plot of the electric potential, electric field, total charge density and total force corresponding to the case of a sheath in a negative potential are shown in Fig. 7. It is observed that the width of the sheath near the cathode ($x = 0$) grows over time, and that the direction of the plasma force remains in the negative x-direction. The magnitude of the plasma force density, however, reduces over time. This test case will be revisited later in this paper in order to examine the effects of a positive sheath and an oscillating sheath on the plasma force density.

B. DC Glow Discharge

The code is next validated by calculating the plasma conditions in a DC glow discharge in N_2 at a pressure of 5 torr. The cathode is grounded, while the potential applied to the anode is determined by solving the circuit equation

$$\Phi_{applied} = \Phi_{ext} - I\,R \tag{24}$$

with the external voltage (Φ_{ext}) is set to 2 kV and the resistance (R) taken to be 300 kΩ. Secondary ionization at the cathode is allowed with an emission coefficient (γ) of 0.1. The plasma transport and ionization parameters are as given in Ref. 21.

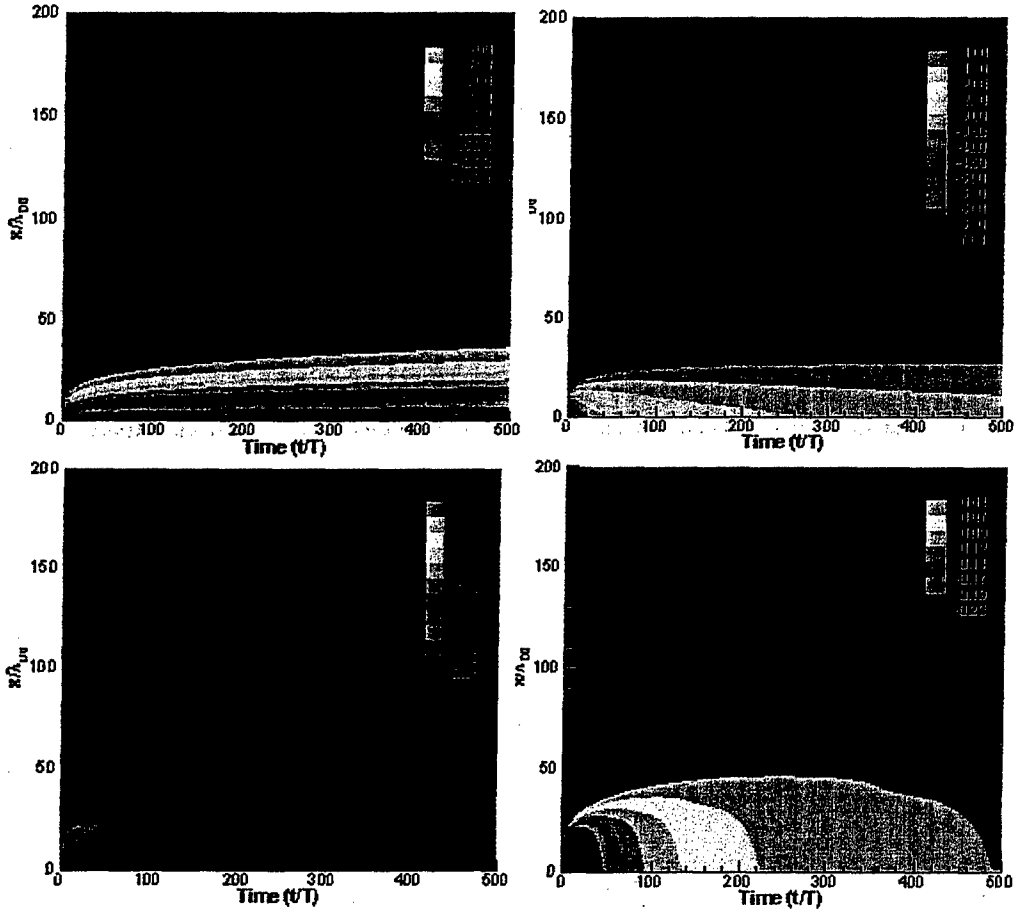

Figure 7. A space-time plot of the electric potential, electric field, total charge density, and total force density corresponding to the case of a sheath in a negative potential. The cathode is located at $x/\lambda_{D0} = 0$, and the effective anode is at $x/\lambda_{D0} = 200$. All quantities have been appropriately non-dimensionalized.

The charged particle number densities, electric potential, and electric field are shown in Fig. 8a. A large region of positive space charge is present near the cathode, which has a thickness of approximately 2 mm. The electric field reaches a maximum in this sheath, with a value on the order of 4 kV/cm. The ion density also reaches a maximum in the cathode sheath, due to the high ionization rate present there resulting from the combined effects of the high electric field and the presence of electrons from cathode emission. Between the cathode and the anode there is a large region of quasi-neutrality, in which the electric field is relatively low (typical value –100 kV/cm). A negative space charge sheath is located near the anode. These characteristics are typical of DC glow discharges in general, and the present simulation is in good agreement with Ref. 30 in particular, which was calculated under the same conditions.

The force density resulting from the DC discharge is shown in Fig 8b. The force density is confined to the sheath regions, with the force near the cathode (where a large electric field and charge density difference are present) much larger than the force near the anode. In both cathode and anode sheath regions, the total force density is due almost entirely to the electric field and is directed towards the respective electrode.

C. RF Glow Discharge

A third test case of the computational code is that of an RF discharge, with the working gas being Helium at a pressure of 1 torr.[22] The purpose of this test case is to ensure the proper behavior of the code in ionizing gases, correct treatment of applied voltages at high frequency, and proper inclusion of the boundary conditions at electrodes, including secondary ionization.

The right electrode is grounded while the potential on the left electrode oscillates sinusoidally with a maximum amplitude of 500V and a frequency of 10 MHz. The distance between electrodes is 4 cm (Fig. 9).

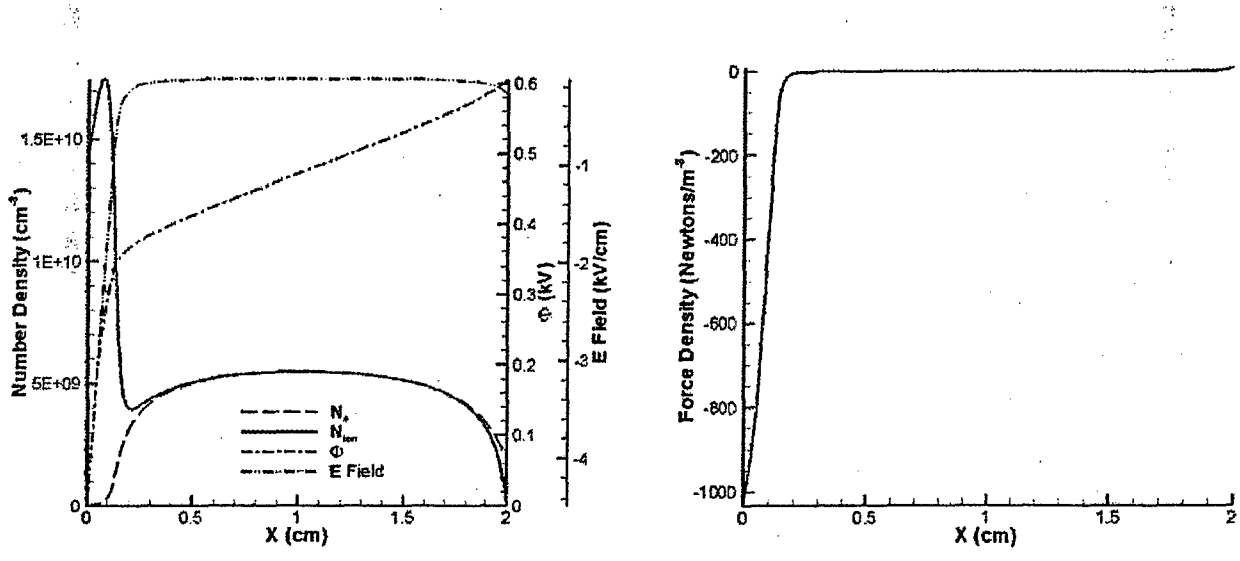

(a) Plasma conditions (b) Force density

Figure 8. Results from a DC glow discharge in N_2 at a pressure of 5 torr.

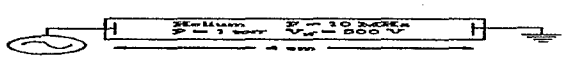

Figure 9. Geometry for the RF discharge used in test case 2.

Initially, the electron and ion densities are uniform and set to 10^{15} m^{-3} everywhere. The electric potential is also uniform and set to 0 V. Electron and ion transport coefficients for Helium are as given by Boeuf[22] and Ward[31]. The electron (and ion) source term is also given by Ref. 31. The solution procedure is to iteratively solve the electron and ion continuity equations, followed by the Poisson equation. This procedure is repeated until a stationary state is achieved in which the periodic form of the solution repeats with every RF cycle. In practice, the solution takes several hundred periods to converge as such.

Converged values of the electron and ion number densities, as well as the electric field are shown in Fig. 10 at four specific points within the RF cycle. Note that at 10 MHz, the ion distribution remains essentially stationary, with changes in the electron distribution being limited to the sheath regions. The agreement between these results and that of Ref. 22 (Fig. 1) is good.

As a further check of the simulation, the electron and ion conduction current and the displacement current on the left electrode are followed in time and compared to those of Ref. 22. The comparison is shown in Fig. 11; again, agreement is good.

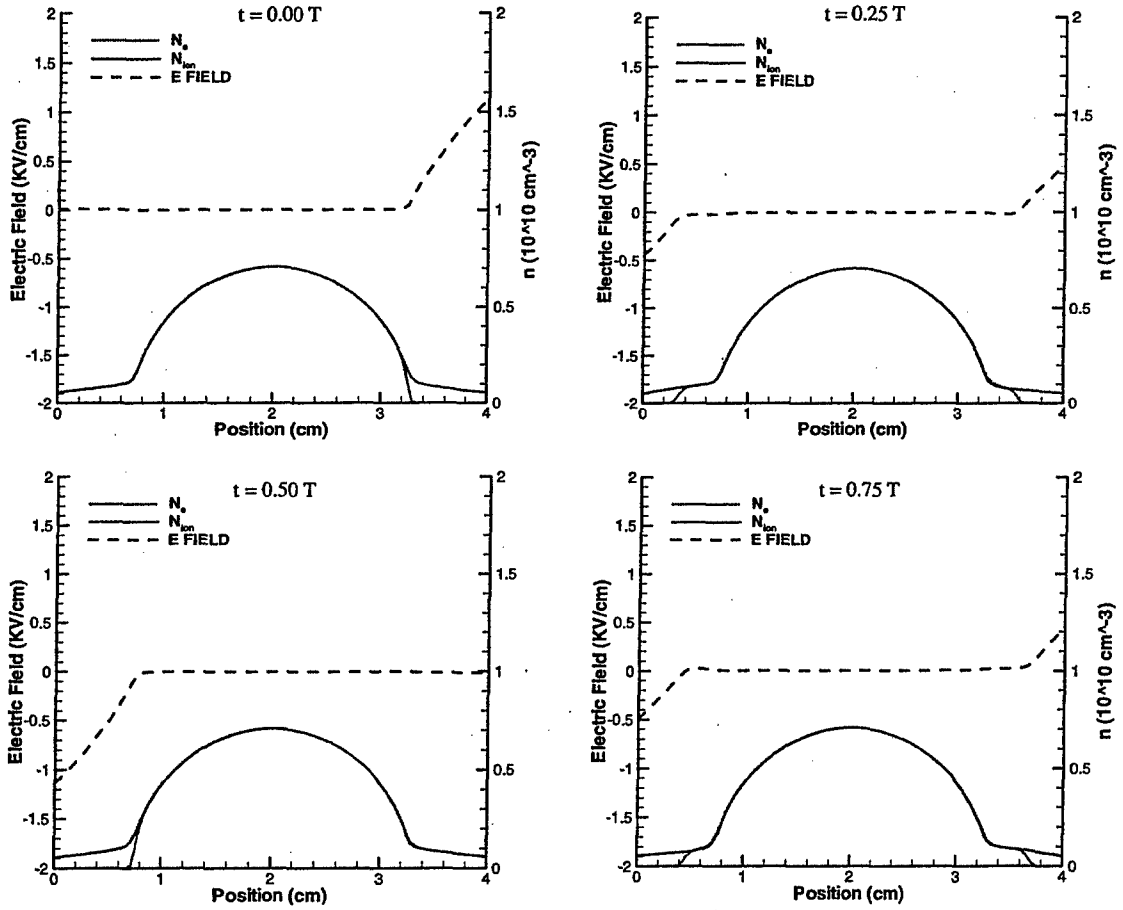

Figure 10. Electron and ion density, along with the corresponding values of the electric field, at four separate points in the RF cycle of a 1 torr Helium discharge at 10 MHz.

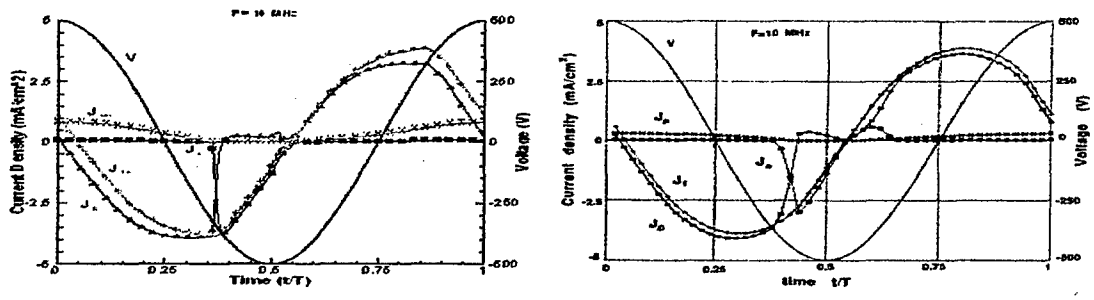

Time variations of current densities and applied potential at the left electrode

(a) Present calculation (b) Previous calculation (Ref. 22)

Figure 11. Time variation of the electron (J_e), positive ion (J_{ion}), displacement (J_D) and total (J_{Tot}) current densities on the left electrode of a 1 torr Helium RF discharge at 10 MHz. The present work is shown in (a); computational results from Ref. 22 in (b).

V. Results and Discussion

Having derived an expression for the plasma force density and ensuring the code is working properly, we next apply the simulation capability to a series of test problems in order to examine the behavior of the plasma force.

A. Transient Sheath for a Positive Potential

The sheath in a non-ionizing Argon plasma at a pressure of 100 torr is reexamined for the case in which the sheath is located within a positive potential (i.e., one in which the sheath is located in a potential that is higher than that of the bulk plasma). The Argon transport parameters remain the same as those used previously. The left boundary of the domain is an electrode, initially at a potential of 0 V. The right boundary models a free plasma region a distance of 200 Debye lengths (based on the unperturbed bulk plasma) from the left boundary. The electron and positive ion densities are initially spatially uniform, while the electric potential is initially zero throughout the domain. At time $t=0$ the left electrode is instantaneously brought to a nondimensional potential of $e\Phi/k_B T_e = +50$. The sudden application of a positive potential draws the highly mobile electrons towards the anode, while the positive ions are repulsed away from the anode. The charge density, potential and electric field at $t/t_{mp} = 100$ are shown in Fig. 12a. Near the anode the electric field is large and positive and there is a region of net negative charge. This field acts to drive electrons to the left and ions to the right. Thus, ions at the right edge of the computational domain are lost to the bulk plasma, while electrons in the bulk plasma are added to the computational domain. The ions are not nearly as mobile as the electrons, thus the formation of the sheath occurs much more slowly than it did for the case of a sheath in a negative potential.

The corresponding force densities for the same moment in time are shown in Fig. 12b. Note that all components of the plasma force on the neutral gas are in the negative x-direction, just as in the case of a sheath in a negative potential. That is, although the sign of the potential applied at the electrode has changed, the direction of plasma force on the neutral gas has not.

Space-time plots of the electric potential, electric field, total charge density and total force corresponding to the case of a sheath in a positive potential are shown in Fig. 13. It is observed that the width of the sheath near the anode ($x/\lambda_{D0} = 0$) grows over time, and that the direction of the plasma force remains in the negative x-direction. The plasma force is concentrated near the electrode, just as for the sheath in a negative potential. The magnitude of the plasma force is reduced over time, illustrating the transient nature of the plasma sheath.

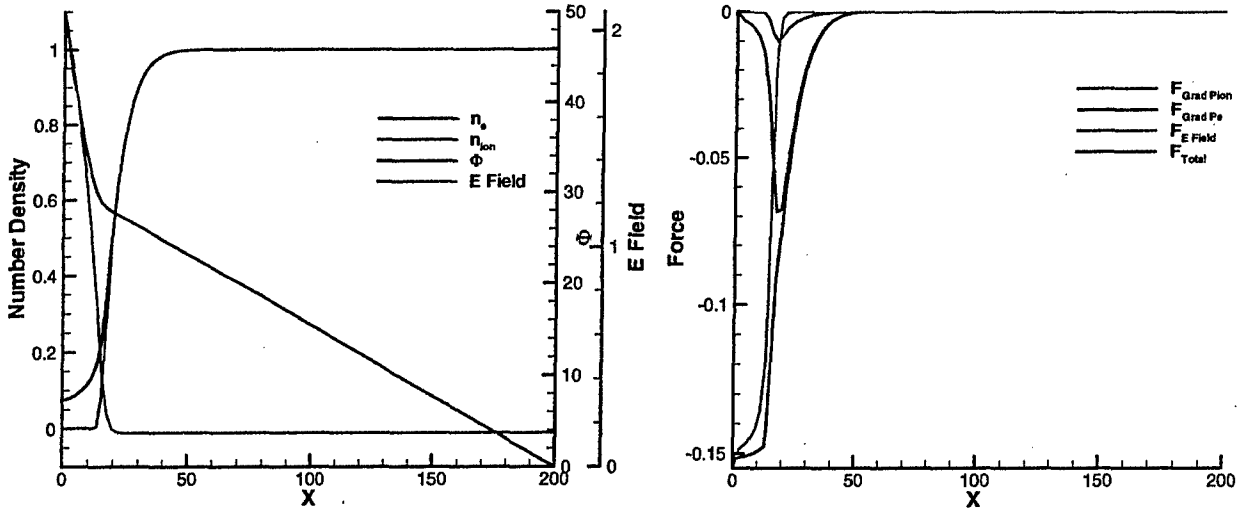

(a) Number densities, potential, and E-field (b) Force density components

Figure 12. Results from a plasma sheath in a positive potential at 100 time units. All quantities have been appropriately nondimensionalized.

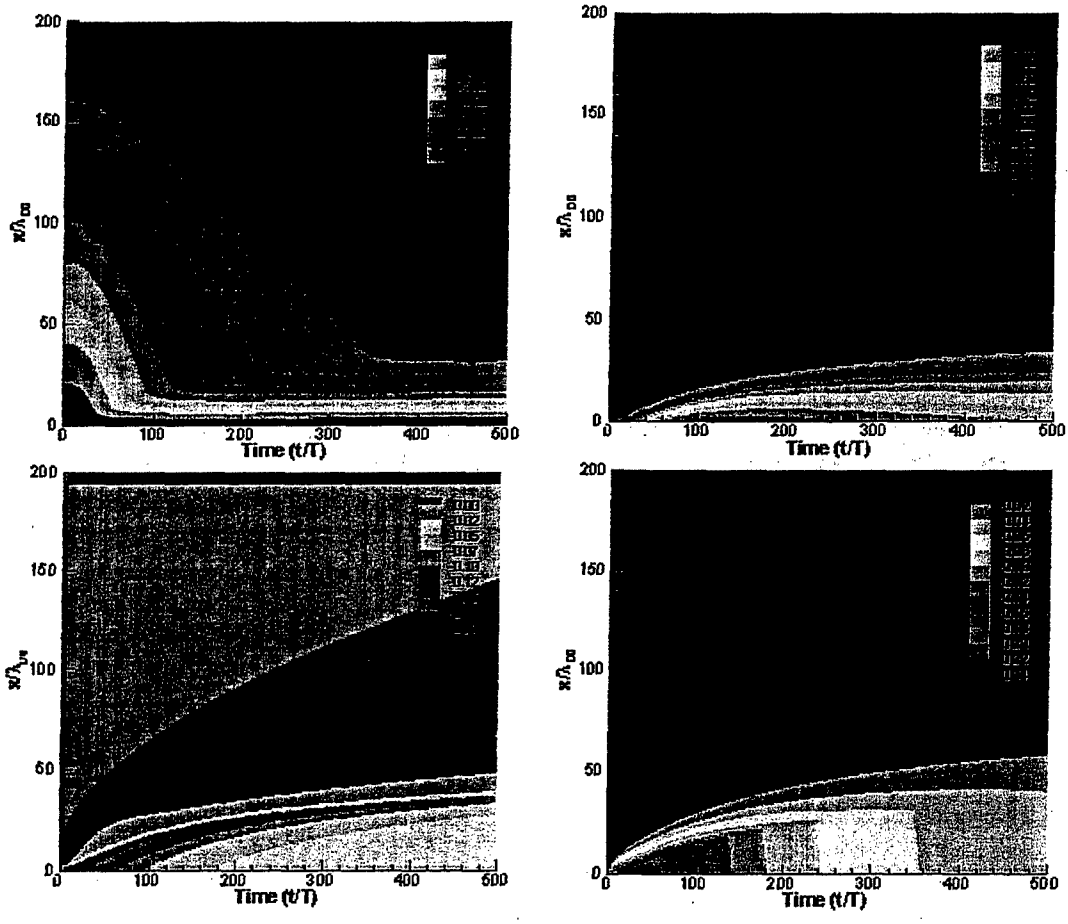

Figure 13. A space-time plot of the electric potential, electric field, total charge density and total force density corresponding to the case of a sheath in a positive potential. The anode is located at $x/\lambda_{D0} = 0$ and the effective cathode is at $x/\lambda_{D0} = 200$. All quantities have been appropriately non-dimensionalized.

B. Transient Sheath for an Oscillating Potential

Having examined the behavior of the plasma sheath in both a negative and a positive potential, it is interesting to examine the case in which the applied potential on the electrode varies sinusoidally. In this case, the nondimensional potential on the electrode is defined as

$$\phi(0,t) = 50\sin(2\pi\nu t) \tag{25}$$

with $\nu = 5\,\text{kHz}$, a typical operating frequency for a DBD. Space-time plots of the electric potential, electric field, total charge density, and total force density are shown in Fig. 14. In these plots time has been nondimensionalized by the oscillation period length (0.2 ms). It is observed that while the potential, electric field, and total charge density alternate between being positive and negative with each half-cycle, the plasma force always remains of the same sign. As in the previous cases, the plasma force is concentrated near the electrode, and rapidly diminishes in magnitude with time.

Caution must be extended if one attempts to directly apply these results to the case of a DBD. There are numerous differences between this simple test case and an actual DBD: in the present case the model is 1D, a dielectric barrier is not present, only the spatial region near one electrode is modeled, and the voltage is quite low. Additionally, the right hand side of the computational domain in this model is open (i.e., charged particles are free to enter or leave the domain according to the local electric field), and a truly periodic solution is not observed. Nevertheless, some insight can be gained by examining the plasma behavior in this simple model. Notice that (after the initial transient) the plasma force "pushes" the neutral gas twice each period; once with a small "push" and again with a larger "push". The larger push is associated with regions of net positive charge, indicating that it is the heavy ions that are primarily responsible for transferring the force of the plasma to the neutral gas.

C. Microdischarges without a Dielectric Barrier

Electrical breakdown in gases at atmospheric pressure normally occurs through a large number of individual breakdown channels, known as microdischarges.[32] Many researchers have studied these microdischarges, including Dhali (et al, Ref. 21), who examined their properties in the absence of a dielectric barrier. Their two-dimensional simulation is repeated here in one-dimension, for the case of a microdischarge in N_2 at atmospheric pressure. The physical processes of ionization (α), recombination (β), diffusion (D) and drift (mobility μ) are included, with corresponding coefficients given as

$\alpha = 5.7\,P\exp(-260P/E)$ cm^{-1} (with pressure P given in torr and electric field E given in V/cm)

$\beta = 1\times10^{-14}$ m^3/s

$\mu_e = 3.8158\times10^{-2}$ $\text{m}^2\,\text{V}^{-1}\,\text{s}^{-1}$ $\quad D_e = 1.8000\times10^{-1}$ m^2/s

$\mu_i = 3.4211\times10^{-4}$ $\text{m}^2\,\text{V}^{-1}\,\text{s}^{-1}$ $\quad D_i = 2.3815\times10^{-5}$ m^2/s

Dhali simulated the physical process of photoionization by placing a homogenous density of neutral background ionization throughout the domain. This was not performed in the present work.

The device to be simulated consists of two plane parallel electrodes a distance of 5 mm apart, with the left electrode grounded and the right electrode held at a potential of 26 kV. As an initial condition the electrons and ions are Gaussian distributed, centered on the cathode with a $1/e$ point of 0.27 mm. The electric field is initially uniform and equal to –52 kV/cm.

During the first few nanoseconds an anode-directed streamer is observed in which the charged particle growth is governed by Townsend's first ionization coefficient (Fig. 15a). In the case of the anode-directed streamer, the normal drift of the electrons is such that they naturally move in the same direction as the streamer, while the positive ions move in the opposite direction. This results in a net negative charge at the streamer head, as illustrated in Fig. 16a, taken at 2 ns. This net charge density, in effect, shifts the cathode closer to the anode, increasing the electric field near the streamer head. Thus, the streamer propagates into an ever-decreasing electric field, which serves to both increase the ionization at the head as well as the velocity, as evident in Fig. 15a.

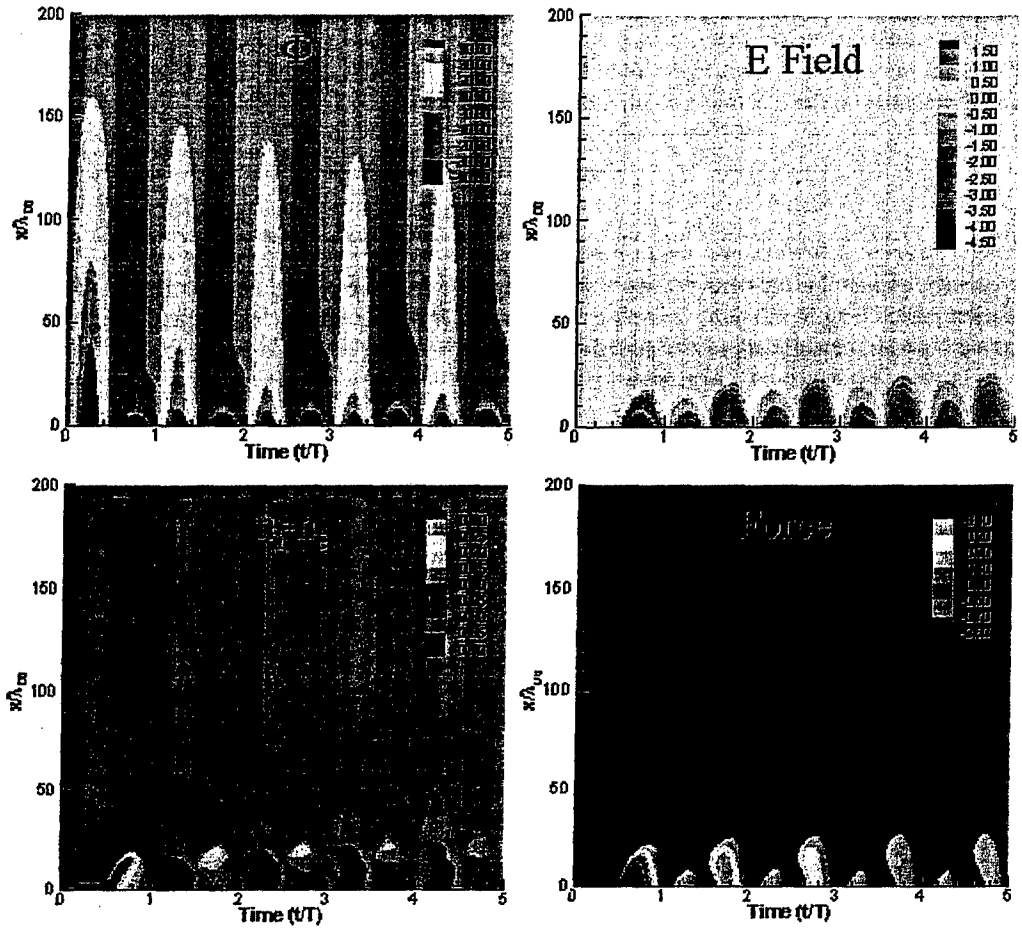

Figure 14. A space-time plot of the electric potential, electric field, total charge density and total force density corresponding to the case of a sheath in an oscillating potential. All quantities have been appropriately non-dimensionalized.

The streamer current (Fig. 15b) initially decreases as the electrons and ions in the initial Gaussian distribution redistribute themselves in order to cancel out the applied electric field. The time scale for this process is of the order of a few tens of dielectric relaxation times, as given by Eq. (22). The exponential rise in the current at later times is indicative of Townsend ionization in the main streamer body.

This streamer crosses the discharge gap in approximately 5 ns, resulting in an average speed on the order of 9.8 x 10^5 m/s. If we take the average value of the electric field at the streamer head as it crosses the gap to be –78 kV/cm (a value determined by tracking the calculation in time), then the average electron drift velocity at the streamer head will be approximately 3.0 x 10^5 m/s, or more than three times slower than the streamer velocity.

Space-time plots of the electric potential (kV), electric field (kV/cm), total charge density (cm^{-3}), and force density (N/cm^3) corresponding to a microdischarge in N_2 at atmospheric pressure are shown in Fig. 17. The non-zero force density is almost entirely localized near the streamer head, and in contrast to previous cases, is positive throughout the domain. That is, the force is continuously directed towards the anode, even when the streamer is far from the anode. This is due to the large negative electric field that exists at the streamer head, combined with the net negative space charge that is also present there. The positivity of the force indicates that, on a time scale characteristic of a microdischarge, electron-neutral collisions are the dominant mechanism for transferring momentum from the plasma to the neutral gas. For example, in the time it takes for the microdischarge to traverse the entire gas gap (5 mm), the heavy ions, with their much lower mobility, will have moved a distance of the order of 0.02 mm, at most (assuming an average electric field of –78 kV/cm, as determined previously). The actual

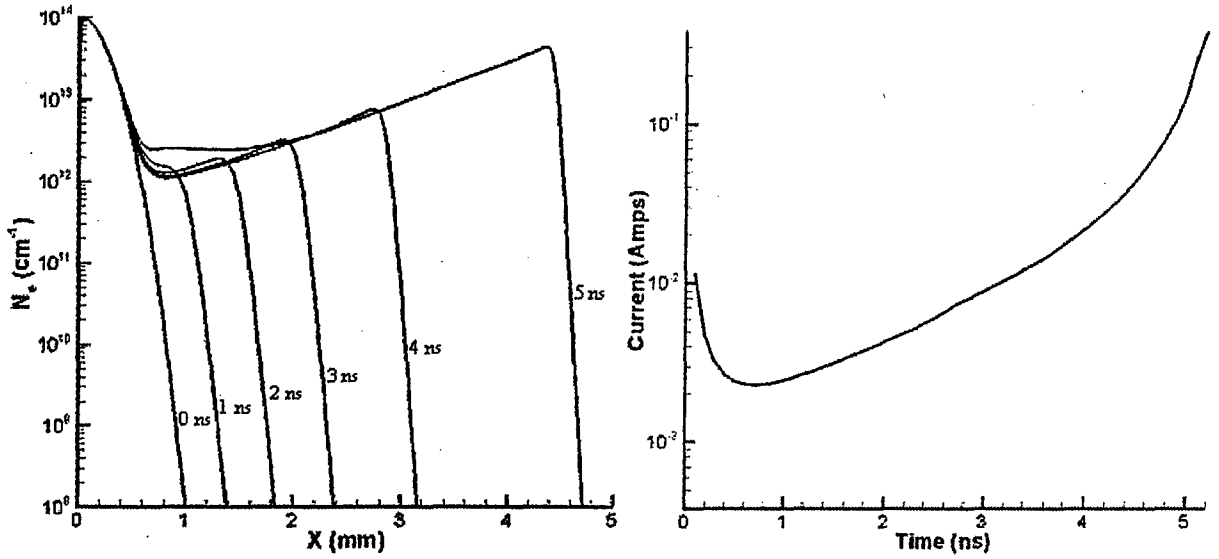

(a) Electron density (b) Current

Figure 15. Profiles of electron density (a) and current (b) for a microdischarge in N_2 at atmospheric pressure. The applied voltage on the anode (located at x = 5 mm) is fixed at 26 kV and the initial charged particle densities are Gaussian distributed, centered on the cathode with a $1/e$ point of 0.27 mm.

distance traveled by the ions during this time will be much less than this because, unlike the electrons at the streamer head which naturally move in a direction of a greater electric field, the ions will move toward the "back side" of the streamer, which is a region of much reduced (in magnitude) electric field (see Fig. 16).

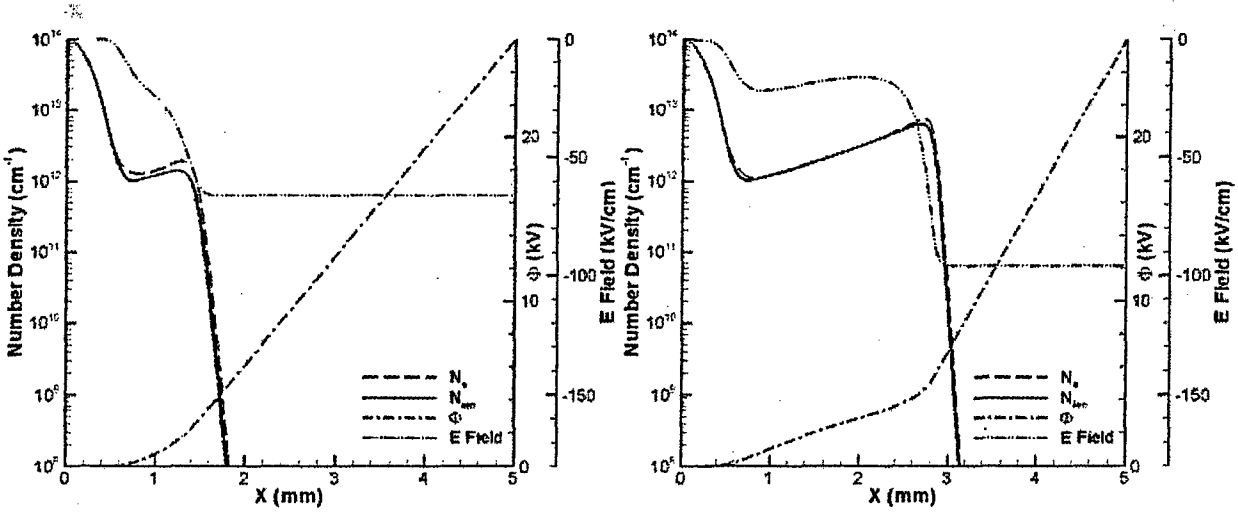

(a) $t = 2$ ns (b) $t = 4$ ns

Figure 16. Profiles of particle density, potential and electric field for a microdischarge in N_2 at atmospheric pressure at (a) 2 ns and (b) 4 ns. These times correspond to an anode-directed streamer and a cathode-directed streamer, respectively. The applied voltage on the anode (located at x = 5 mm) is fixed at 68 kV and the initial charged particle densities are Gaussian distributed, centered on the cathode with a $1/e$ point of 0.27 mm.

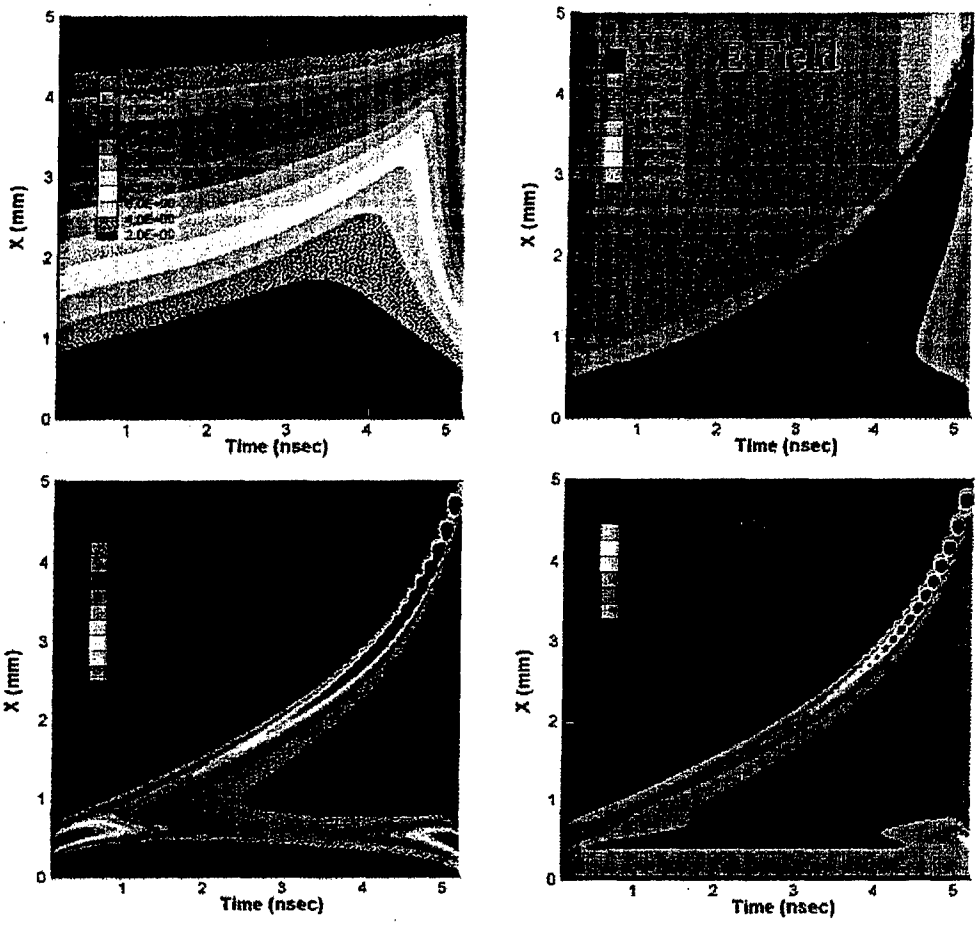

Figure 17. Space-time plots of the electric potential (kV), electric field (kV/cm), total charge density (cm^{-3}) and, total force density (N/m^3) corresponding to a microdischarge in N_2 at atmospheric pressure. The cathode is at x = 0 mm, the anode at x = 5 mm, and the applied potential is 68 kV.

VI. Conclusion

Several simulations have been made of various plasma devices. These simulations are based on successive numerical solutions of the electron and ion charge conservation equations (in the drift-diffusion approximation) coupled with Poisson's equation. The code was validated with three test problems, illustrating its ability to correctly solve the governing equations, and then applied to several simple problems to examine the behavior of the resulting force density. Future work will consist of extending the model to higher dimensions, examining the effect of negative ions (present in air plasmas), and optimization studies involving electrode geometry, dielectric permittivity and applied voltage waveform.

Acknowledgments

The authors are grateful for AFOSR sponsorship under a task monitored by Dr. J. Schmisseur, and acknowledge useful conversations with M. Kushner, D. Gaitonde, J. Poggie, J. Shang, W. Bailey, T. McLaughlin, L. Enloe and T. Corke.

References

[1] J. Reece Roth, "Aerodynamic Flow Acceleration Using Paraelectric and Peristaltic Electrohydrodynamic Effects of a One Atmosphere Uniform Glow Discharge Plasma (OAUGDP™)," *Physics of Plasmas*, Volume 10, Number 5 (2003).

[2] Lennart S. Hultgren and David E. Ashpis, "Demonstration of Separation Delay with Glow-Discharge Plasma Actuators," Technical Paper 2003-1025 (AIAA Press, Washington DC, 2003).

[3] Martiqua L. Post and Thomas C. Corke, "Separation Control on High Angle of Attack Airfoil Using Plasma Actuators," Technical Paper 2003-1024 (AIAA Press, Washington DC, 2003).

[4] C.L. Enloe, et al, "Mechanisms and Responses of a Single Dielectric Barrier Discharge", Technical Paper 2003-1021 (AIAA Press, Washington DC, 2003).

[5] J. Reece Roth, Daniel M. Sherman and Stephen P. Wilkinson, "Electrohydrodynamic Flow Control with a Glow-Discharge Surface Plasma," *AIAA Journal*, Vol 38, No. 7 (2000).

[6] J. Reece Roth, Daniel M. Sherman and Stephen P. Wilkinson, "Boundary Layer Flow Control with a One Atmosphere Uniform Glow Discharge Surface Plasma," Technical Paper 98-0328 (AIAA Press, Washington DC, 1998).

[7] Luc Leger, Eric Moreau and Gerard Touchard, "Electrohydrodynamic Airflow Control Along a Flat Plate By a DC Surface Corona Discharge – Velocity Profile And Wall Pressure Measurements," Technical Paper 2002-2833 (AIAA Press, Washington DC, 2002).

[8] L. S. Hultgren and D.E. Ashpis, "Demonstration of Separation Delay with Glow-Discharge Plasma Actuators," Technical Paper 2003-1025 (AIAA Press, Washington DC, 2003).

[9] Robert Sierakowski, Chief Scientist, AFRL/MN, Private Communication (Sep 2003).

[10] J. Reece Roth, Daniel M. Sherman and Stephen P. Wilkinson, "Boundary Layer Flow Control with a One Atmosphere Uniform Glow Discharge Surface Plasma," Technical Paper 98-0328 (AIAA Press, Washington DC, 1998).

[11] Martiqua L. Post and Thomas C. Corke, "Separation Control Using Plasma Actuators – Stationary and Oscillating Airfoils," Technical Paper 2004-0841 (AIAA Press, Washington DC, 2004).

[12] Nicholas A. Krall and Alvin W. Trivelpiece, *Principles of Plasma Physics*, San Francisco Press, Inc., San Francisco CA, 1986.

[13] Dieter Braun, Ulrich Kuchler and Gerhard Pietsch. "Microdischarges in Air-Fed Ozonizers," *Journal of Physics D: Applied Physics*, Vol 24, 1991, pp 564-572.

[14] Baldur Eliasson. "Modeling and Applications of Silent Discharge Plasmas," *IEEE Transactions on Plasma Science*, Vol 19, No 2, April 1991, pp 309-323.

[15] Dieter Braun, Valentin Gibalov and Gerhard Pietsch. "Two-dimensional Modeling of the Dielectric Barrier Discharge in Air," *Plasma Sources Science Technology*, 1 (1992), pp. 166-174.

[16] Jing Li and Shirshak K. Dhali, "Simulation of Microdischarges in a Dielectric-Barrier Discharge," *Journal of Applied Physics*, 82 (9), 1 November 1997, pp 4205-4210.

[17] Gunther Steinle, Doerte Neundorf, Wolfgang Hiller and Martin Pietralla. "Two-dimensional Simulations of Filaments in Barrier Discharges," *Journal of Physics D: Applied Physics*, 32 (1999), pp 1350-1356.

[18] Rami B. Gadri. "One Atmosphere Glow Discharge Structure Revealed by Computer Modeling," *IEEE Transactions on Plasma Science*, 27 (1), February 1999, pp 36-37.

[19] Valentin I Gibalov and Gerhard J. Pietsch. "The Development of Dielectric Barrier Discharges in Gas Gaps and on Surfaces," *Journal of Physics D: Applied Physics*, 33 (2000), pp 2618-2636.

[20] C.L. Enloe, Thomas E. McLaughlin, Robert D. VanDyken, K.D. Kachner, Eric J. Jumper, Thomas C. Corke, and O. Haddad, "Mechanisms and Responses of a Single Dielectric Barrier Plasma Actuator: Geometric Effects," *AIAA Journal*, Vol. 42, No. 3, March 2004.

[21] S.K. Dhali and P.F. Williams, "Two-Dimensional Studies of Streamers in Gases," *Journal of Applied Physics*, Volume 62, Number 12, 15 December 1987, pp 4696-4707.

[22] J.P. Boeuf, "Numerical Model of RF Glow Discharges," *Physical Review A*, Volume 36, Number 6, 15 September 1987, pp 2782-2792.

[23] D.L. Scharfetter and H.K. Gummel, "Large-Signal Analysis of a Silicon Read Diode Oscillator," *IEEE Transactions on Electron Devices*, Vol. ED-16, No 1, January 1969, pp 64-77.

[24] F.H. Harlow and J.E. Welch, "Numerical Calculation of Time-Dependent Viscous Incompressible Flow of Fluid with Free Surface," *Physics of Fluids*, Volume 8, p 2182 (1965).

[25] W.H. Press, B.P. Flannery, S.A. Teukolsky, and W.T. Vetterling, *Numerical Recipes: The Art of Scientific Computing*, Cambridge University Press, New York NY, 1989.

[26] Yu. B. Golubovskii, V.A. Maiorov, J. Behnke, and J.F. Behnke, "Influence of Interaction Between Charged Particles and Dielectric Surface Over a Homogeneous Barrier Discharge in Nitrogen," Journal of Physics D: Applied Physics, 35, (2002), pp. 751-761.

[27] A. Fiala, L.C. Pitchford, and J.P. Boeuf, "Two-Dimensional, Hybrid Model of Low-Pressure Glow Discharges," *Physical Review E*, Volume 49, Number 6, June 1994, pp 5607-5622.

[28] J.P. Bouef and A. Merad, "Fluid and Hybrid Models of Non-Equilibrium Discharges," *Plasma Processing of Semiconductors*, edited by P.F. Williams, Kluwer Academic Publishers, The Netherlands, 1997, pp. 291-319.

[29] J. Poggie and D.V. Gaitonde, "Electrode Boundary Conditions in Magnetogasdynamic Flow Control," Technical Paper 2002-0199 (AIAA Press, Washington DC, 2002).

[30] J. Poggie, "Numerical Exploration of Flow Control with Glow Discharges", Technical Paper 2004-2658 (AIAA Press, Washington DC, 2004).

[31] A.L. Ward, "Calculations of Cathode-Fall Characteristics," *Journal of Applied Physics*, Volume 33, p 2789 (1962).

[32] U. Kogelschatz, "Fundamentals and Applications of Dielectric-Barrier Discharges," May 2000.